Direct Top-Down Fabrication of Large-Area Graphene Arrays by an In Situ Etching Method

*Dechao Geng, Huaping Wang, Yu Wan, Zhiping Xu, Birong Luo, Jie Xu, and Gui Yu**

Due to its spectacular electronic properties,[1–4] graphene is emerging as a promising new material for next-generation electronics. It has been predicted that graphene-based field-effect transistors and conductive interconnects with high mobility of charge carriers could be central parts for future electronic circuits.[5] Considering that monolayer graphene is zero-band, band-engineering is of great significance for further wide applications. Theoretical calculations have indicated that, depending on the size, shape, and edge structure, graphene should display a variety of properties.[6,7] Thus many graphene structures have been fabricated for tuning graphene properties. Of particular interest would be the construction of atomically precise graphene nanoribbons, in which charge carriers are confined in the lateral dimension whereby the electronic properties are controlled by the width and specific crystallographic orientation of the ribbon, posing potential application in spintronic devices.[8] Based on all these promising applications, proper micro or nanoengineering for tailoring graphene sheets into desired shapes with specific dimensions is highly required.

Mask-protected electron beam lithography patterning technique has been extensively employed to prepare large-scale aligned graphene micro or nanostructures.[9–12] However, the whole process is rather complicated and time-consuming. Another drawback is that residues left derived from fabrication can significantly affect charge transport and further lower device performance. Several metallic nanoparticles were reported as etchant for highly oriented pyrolytic graphite nanocutting,[13–15] in which the etching process occurred along crystallographic direction. Such technique could be served as an efficient approach to produce graphene nanostructures with well-defined edges. However, the controllability of the method is not high and the scalability is also largely limited.

Recently, Zhou and Geng reported the in situ anisotropic and fractal etching of chemical vapor deposited graphene, respectively.[16,17] Following a certain crystallographic orientation, the chemical vapor deposition (CVD)-grown graphene was etched by hydrogen into regular hexagonal holes or complicated fractal patterns. Other work on hydrogen etching effects toward graphene structures has also been carried out.[18–21] However, it is still far from applications, while the location and orientation of remaining graphene pieces could not be precisely controlled. In short, to date, directly producing large-scale graphene structures with precise control on shape, size, and location is still an extremely challenging task.

In this study, we demonstrate for the first time a CVD process to directly fabricate large-area graphene arrays with full control over the size, shape, and orientation. Precise micro and nanocutting of graphene film and single crystals is realized by introduction of hydrogen gas for in situ etching. Employing the etching approach, we have achieved large-area aligned graphene arrays with single size down to 100 nm and hexagonal shaped features. Further, our experiments together with proposed etching mechanism strongly suggested that a reaction-controlled mode is responsible for the production of hexagonal graphene arrays, providing a generally effective approach for engineering of graphene and other 2D materials.

To prepare sub-micrometer graphene arrays, we first started by preparing graphene film and hexagonal graphene crystals on liquid Cu surface by ambient pressure CVD. It is reported that the liquid Cu could be a particularly effective catalyst in making uniform monolayer graphene film and large-size graphene single crystals.[22] As for the whole CVD process, briefly, a Cu/W substrate was heated to a temperature higher than the melting point of Cu (1084 °C; we performed temperatures in the range 1100–1200 °C) and then annealed for 60 min in pure H_2 atmosphere. A monolayer graphene film or hexagonal graphene single crystals were then grown using CH_4 in Ar/H_2 as the carrier gas. In these growth cases, the monolayer graphene film was grown on a liquid Cu surface using CH_4 at 0.7 standard cubic centimeters per minute (sccm), 30 sccm H_2, and 1500 sccm Ar for 60 min at 1140 °C, while only shortening time to 40 min could assure the growth of graphene single crystals (Figure S1, Supporting Information). In the case of in situ etching experiments, after graphene growth, the CH_4 source was turned off and the Ar/H_2 flow was continued for a period of time at a particular flow rate ratio while keeping the temperature the same. Finally, after the etching stage, the furnace was opened, allowing the system to cool rapidly to room temperature. The detailed CVD conditions of graphene growth and etching are listed in Table S1 (Supporting Information). The whole process is illustrated schematically in **Figure 1**.

As for the in situ etching of large-area monolayer graphene film, it was clearly found, as shown in **Figure 2**a that a large amount of graphene flakes with micrometer size were dispersed

D. Geng, H. Wang, Dr. B. Luo, J. Xu, Prof. G. Yu
Beijing National Laboratory for Molecular Sciences
Institute of Chemistry
Chinese Academy of Sciences
Beijing 100190, PR China
E-mail: yugui@iccas.ac.cn

D. Geng, H. Wang, J. Xu
University of Chinese Academy of Sciences
Beijing 10049, PR China

Y. Wan, Prof. Z. Xu
Applied Mechanics Laboratory, Department of Engineering Mechanics and Center for Nano and Micro Mechanics
Tsinghua University
Beijing 100084, PR China

DOI: 10.1002/adma.201501524

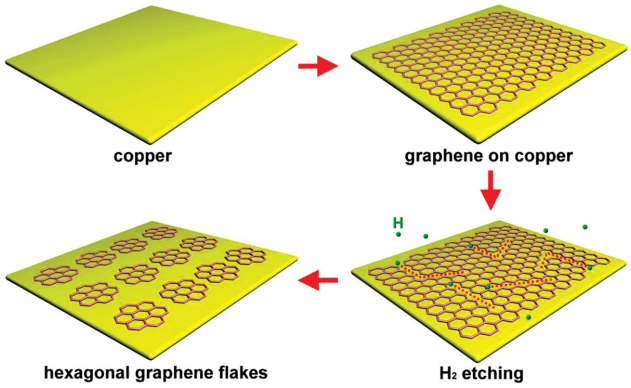

Figure 1. Schematic showing in situ etching process on CVD graphene film for formation of hexagonal graphene arrays.

on the whole Cu surface after keeping the etching stage for 2 h. We observed that the flakes shared the similar size. Size statistics show that the average size falls into the range from 3 to 5 μm (Figure S2, Supporting Information). Further investigation showed that those flakes displayed regular hexagonal shape, the same with graphene single crystals grown on metals[23] by CVD. It is well known that the etching reaction is the reverse process of graphene growth, as hydrogen can react with carbon in graphene and produce methane. On this basis, certain correlation probably exists between the two same shaped graphene flakes, which will be discussed later. For the single graphene flake, systematical characterizations were performed. It was observed that the edges of the etched remaining flakes were sharp (Figure 2b), indicating a uniform atomic orientation. Previous theoretical study revealed that in the graphene gasification reaction, since the C—C bond on the armchair face was the weakest one, it was more amenable to cleavage compared to the C—C bond on the zig-zag face.[16,24,25] Detailed characterization of the atomic configuration is still ongoing for the determination of the edge type. As for the regular flakes, it should be noted that layer number was another critical parameter in engineering graphene properties. The graphene flakes were transferred onto 300 nm SiO_2/Si substrate by the electric-chemical bubbling method. Figure 2c shows the optical microscopy image of large-scale hexagonal flakes. Raman spectrum measurements using a 514 nm excitation laser were conducted to identify the layer number. Figure 2d displays typical Raman spectrum of the transferred graphene flakes. The spectrum is characteristic of single-layer graphene [a symmetric 2D peak located at 2698 cm^{-1} with a full width at half-maximum of 35–40 cm^{-1} and a large intensity ratio of the 2D and G bands (I_{2D}/I_G = 2.5–4)]. A tiny D peak for those graphene flakes was detected due to the edge-effect, in which the size of graphene flakes was comparable or even smaller than that of laser point (≈5 μm). All the data suggested that the as-etched hexagonal flakes owned the same characteristics with original graphene film.

To further investigate the exotic etching behavior of graphene on liquid Cu surface, large-size single-crystal graphene grains were employed. The whole in situ etching process was similar to that of the graphene film as schematically displayed in **Figure 3**a. The etchant H_2 flow rate was kept the same while the etched time was set for 1 h. It was remarkably found that large-scale uniform graphene arrays were etched from the original graphene grain (Figure 3b). All the remaining graphene flakes also displayed typical hexagonal shape, further demonstrating the regular etching rule for graphene. It was noted that the etched-after flakes had similar size, mostly ranging from 1 to 3 μm. After the whole etching process, the outline of original single graphene grain was still maintained, as red marked in Figure 3b. To characterize the as-etched graphene flakes, combination of Raman mapping and transmission electron microscopy (TEM) has been performed. Raman mapping was conducted on the transferred graphene grains (Figure 3c) for more information, in which the intensity mapping of the two characterized peaks G and 2D was clearly shown in uniformity across the whole etched grain while the inconsistency in the D peak mapping because of edge-effect (Figure 3d–f). The typical intensity ratio (I_{2D}/I_G) within a flake was larger than 2, indicating that our samples are single-layer graphene.

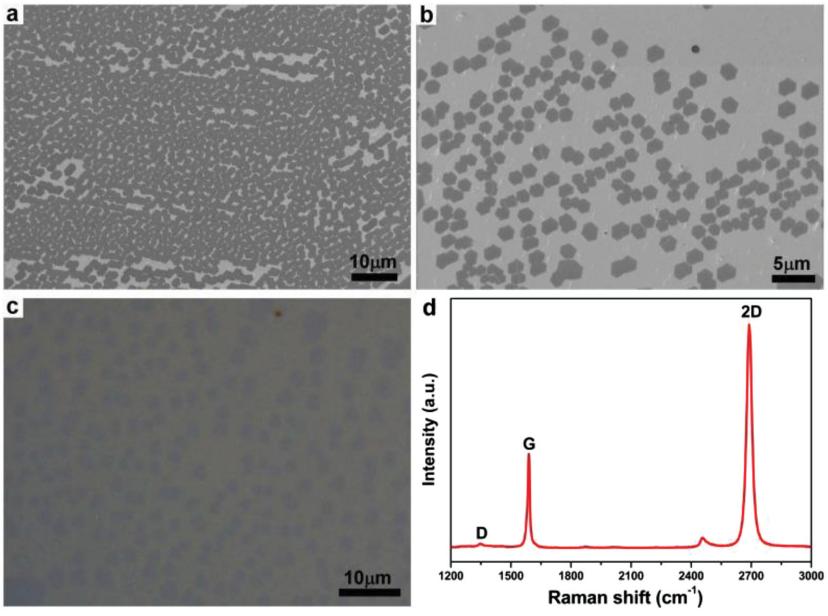

Figure 2. a,b) SEM images of the graphene flakes obtained by etching graphene films. c) Optical image of the transferred graphene arrays onto 300 nm SiO_2/Si substrates. d) Typical Raman spectrum of single graphene flake.

Prior to TEM measurements, the electrochemical-assisted method was employed to separate the graphene flakes with Cu. It was easy to locate the as-transferred graphene samples for further characterization (Figure 3g). Then selected-area electron diffraction (SAED) patterns showed the same sixfold symmetric diffraction points at different regions marked 1–4 over the entire graphene flake (Figure 3h–k). The results demonstrated that the remaining hexagonal grain contained no rotational boundaries to within

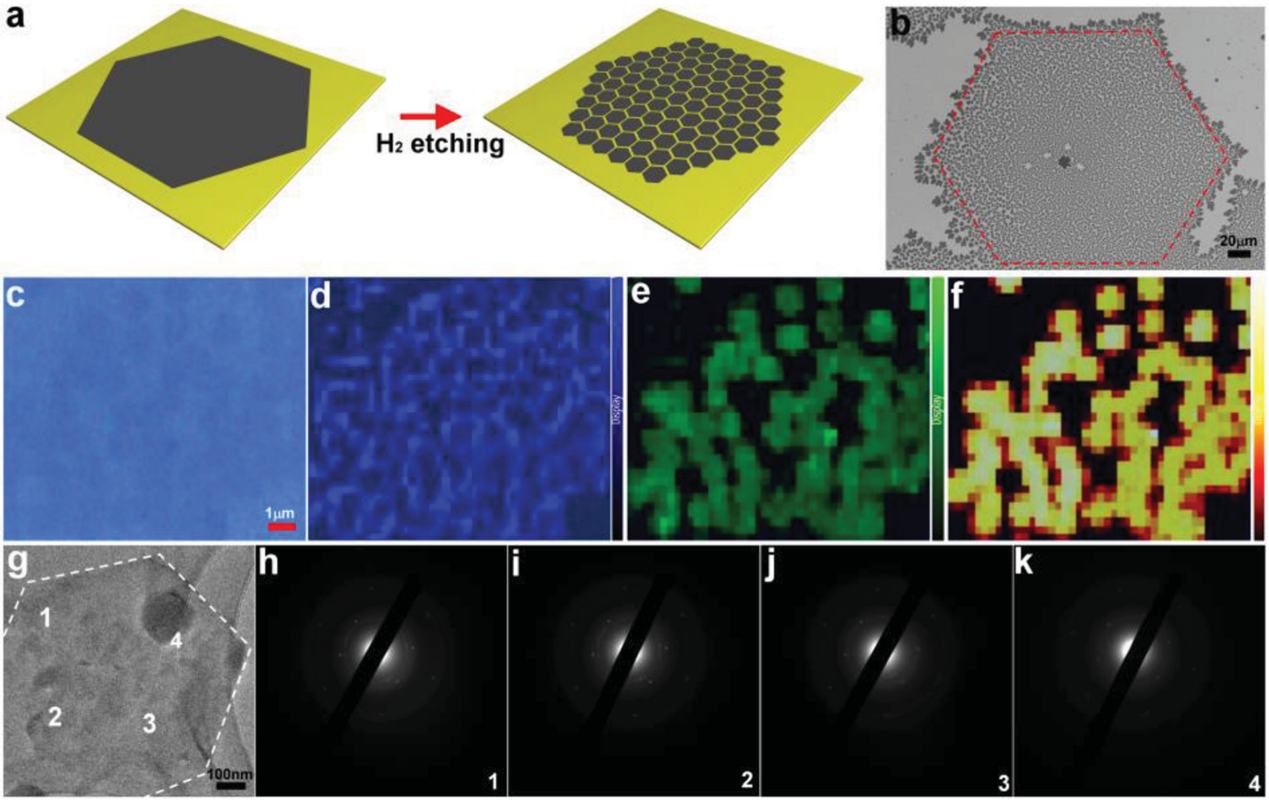

Figure 3. Structure characterizations of the graphene flakes obtained by etching graphene single crystal. a) Schematic diagram of graphene single crystals etching process. b) Typical SEM images of etched large-scale graphene arrays on the copper surface at certain conditions. c) Optical image of the transferred graphene grain onto 300 nm SiO_2/Si substrates. d–f) Intensity mapping of the D, G, and 2D Raman peaks, respectively, for graphene arrays. g) TEM image of the single hexagonal graphene flake on a copper TEM grid. h–k) SAED data for small regions of single flake as indicated 1 to 4.

our measurement accuracy of 0.5°. We have also tested other individual graphene grains and found that all of them show the single-crystalline feature from the SAED results. The diffraction patterns from original graphene single-crystals and etched remaining flakes displayed the same orientation, furthering confirmed the regular etched behavior.

The role of etchant H_2 was fully explored in engineering size of graphene and etched mode. We conducted those experiments on the monolayer graphene film. Different flow rates of H_2 have been employed while the Ar and temperature were kept the same for compare. All the conditions are listed in Table S2 (Supporting Information). In those cases under different H_2 flow rate, the obvious change in etched mode was found. Etching mode followed the fractal rule when the H_2 flow rate fell into 10–40 sccm, while the anisotropic mode played more important role as increasing the H_2 up to 40 sccm and larger. It is suggested that the H_2 flow rate was largely responsible for graphene etching process (Figure S3, Supporting Information). The etched graphene arrays could not be available at large flow rate of H_2 (>40 sccm). While under fractal etching mode with a low H_2 flow rate, increasing the etched time would lead to graphene arrays. On this basis, the etching H_2 range for formation of graphene arrays was set as 10 to 40 sccm.

To understand this etching behavior of graphene on liquid Cu surface, here we provide a theoretical analysis on the pattern formation of etched graphene. In the initial stage of etching, nuclei of etched graphene could form, which expand as the hydrogenation continues. This process replies on the supply of hydrogen molecules on graphene and the expansion of etched area suffers from the point effect of diffusion that amplifies shape fluctuations and leads to shape instabilities beyond a critical size of nucleus. Afterward hydrogen etching processes along the tips of instabilities and is controlled by reaction therein. Initiated by H_2 etchant under certain flow rate (10–40 sccm), the fractal pattern of etched channels branches out after instability occurs (**Figure 4**a), whereas sharp turns are displayed in Figure 4b. The whole process is limited by the hydrogen etching reactions that occur at the advancing front of etching channels. It should be noted that the width of these channels $w = 0.234 \pm 0.050$ μm is found to be quite uniform. This value may be determined by the size of protruded region of graphene during the destabilization of hydrogen etching.

Analysis of the scanning electron microscopy (SEM) data further shows general features of the etched pattern. First, the length of straight segments in the etched pattern varies in a very narrow distribution, centered at $l = 1$ μm (Figure 4c). Second, the angle of sharp turns is 120° (Figure 4d), with variations that might be caused by the wrinkles or local strain in graphene. With this uniformity in the length of straight etching channels and etching angles between them, a hexagonal graphene flakes could be formed after the etching process ends (Figure S4, Supporting Information). The uniformity of straight

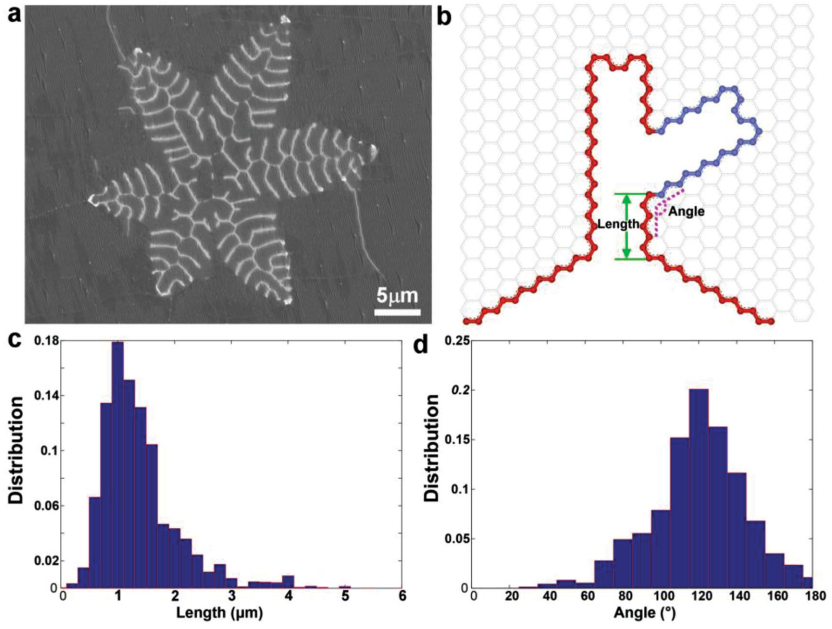

Figure 4. a) SEM image of an etched fractal pattern. b) Illustration of the formation of straight, narrow etching channels (red) and branches (blue) that is biased by 120°. c,d) Distribution of the turning angle at branches and length of straight segments, which are measured from the SEM data.

etching channels could be related to the activation energy barrier to make such a turn. Considering hydrogen etching along the zig-zag edge with step size of 0.246 nm,[13] the 1 μm length of straight segment means the probability for branching is $p = 2.46 \times 10^{-4}$. An Arrhenius analysis of the kinetics predicts the activation barrier $E_a = -k_B T \ln(p \times 10^{-13}) = 4.66$ eV at 1140 °C, which is higher than the energy to remove one carbon atom from graphene that is 0.518–1.853 eV.[13] This high activation energy assures the straightness of etched segments and the formation of regular hexagonal graphene after the etching process.

Moreover, an evolutionary SEM characterization of graphene flake as a function of etching time was conducted as shown in Figure S5 (Supporting Information). It is observed that the etched graphene patterns have an evolutionary change and the hexagonal graphene flakes gradually were formed and eventually resulted in large-area hexagonal graphene arrays. To investigate the effects of the number of etching channels on the graphene, we have performed experiments to give the statistics on density of etching channels during the etching process (Figure S6, Supporting Information). It is clearly found that a higher density of etching channels results in more-hexagonal graphene flakes. The etching selectivity to size has also been studied, whereas the size of as-etched graphene flakes is largely determined by the width of etching channels after the formation of etched network. Then the increase in the width of etching channels leads to gradual decrease in the size of graphene flakes (Figure S7, Supporting Information).

Further control over etching conditions led to precise tuning on the size of etched grains. **Figure 5**a–c shows the large-area etched grains arrays under varied etched conditions as displayed in Table S3 (Supporting Information). It was observed that the size of etched remaining grains gradually decreased as etching time increased. The detailed statistics on the size of graphene arrays (Figure 5d–f) showed that large area sub-micrometer hexagonal graphene arrays could be available. After the top-down fractal etching process, the as-etched graphene flakes owned the same characteristics, including the same morphology and size. Given the quite uniform length and width of etched channels during the etching process, the centers of the etched graphene flakes are expected to be separated at the same distance, leading to the well-adjusted hexagonal graphene arrays. However, it should be noted that the uniformity could be disturbed by various experimental conditions such as the presence of defects (point defects, wrinkles, etc.) in graphene or the substrate, which explains the irregularity in graphene flake patterns in Figure 5a–c. We have used different etching conditions for comparison, while the graphene size could be further controlled. By optimizing the etched process, direct control over the graphene size was ultimately realized. It should be noted that the minimum size of the etched remaining graphene flakes was even down to nanometers. Combination certain etched conditions with prolonged time resulted in creation of large area aligned hexagonal flakes with single size at about 100 nm as shown in Figure S8. (Supporting Information). The etching conditions for goal of graphene nanoengineering are still optimized and it is believed that the nanometer flakes will be successfully produced. Then the direct preparation of graphene quantum dots will be available. Our etching approach indeed provided an effective and facile way for directly making graphene aligned arrays with high control over the size and orientation.

To summarize, we have developed a direct method to fabricate large-scale graphene arrays with control over the size, shape, and location. The in situ etching of chemical vapor-deposited graphene avoids introduction of impurities when comparing with the conventional mask-assisted methods. Through precise tuning of the etching on graphene single-crystals, creation for 100 nm-scale graphene arrays has been realized. The direct etching method will provide a novel guideline for preparation of nanometer graphene quantum dots and possess potential in graphene-based electronics.

Experimental Section

50 μm-thick Cu foil (99.8% purity) and 100 μm-thick W foil (99.95%) were obtained from Alfa Aesar. Several pieces of Cu foils were placed on the W substrate. After samples were put into the 1 in. quartz tube, the whole system was pumped to ≈5 Pa followed by filling the system with H_2. After switching off pumping, the quartz tube is at an ambient pressure with continuous H_2 flow. The furnace was then heated up to a fixed temperature in ≈1 h followed by annealing the substrates for 50–60 min. The growth and etching parts are described in the main text.

Etched remaining hexagonal graphene flakes were transferred to a 300 nm SiO_2/Si substrate by electrochemical method. The samples were characterized by SEM (Hitachi S-4800, 1 kV), TEM (Tecnai G2

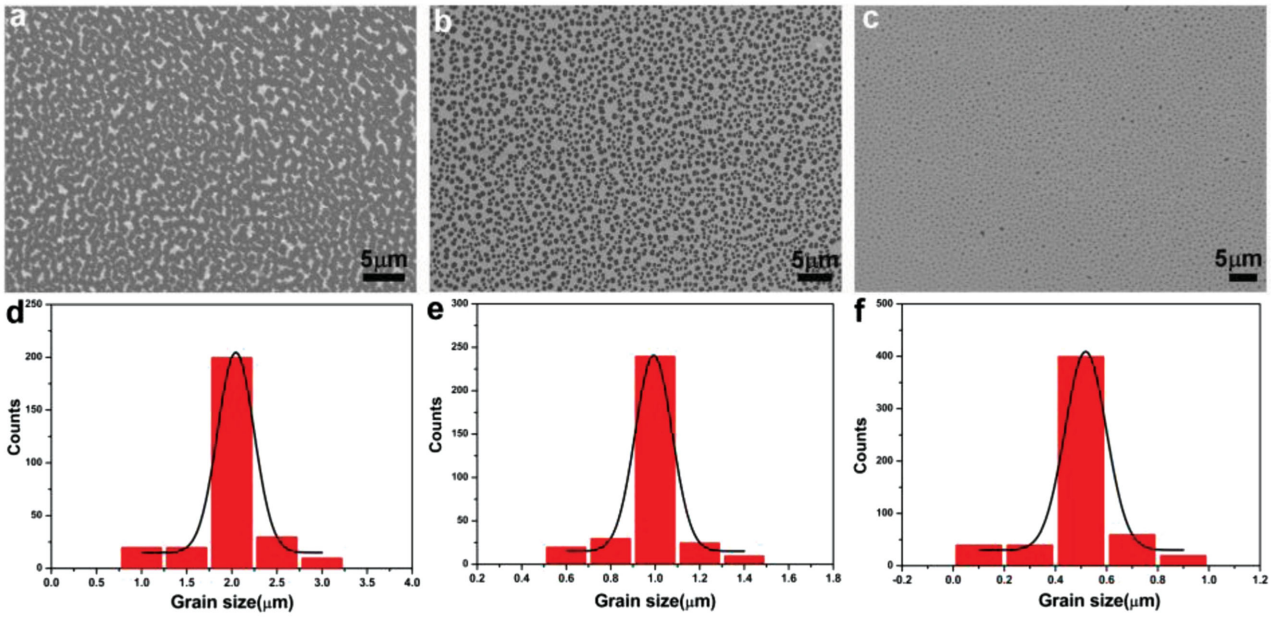

Figure 5. Size-engineering of graphene arrays. a–c) SEM images of etched graphene arrays at different condition as shown in Table S3 (Supporting Information), with the time for 120, 150, and 180 min, respectively. d–f) Size statistics of graphene arrays corresponding to a–c.

F20 U-TWIN transmission electron microscope operated at 200 kV), and Raman spectroscopy (Renishaw inVia Plus, with laser excitation at 514 nm).

Supporting Information

Supporting Information is available from the Wiley Online Library or from the author.

Acknowledgements

D.G. and H.W. contributed equally to this work. This work was supported by the National Natural Science Foundation of China (61390502), the National Major State Basic Research Development Program (2013CB933403 and 2013CBA01602), and the Strategic Priority Research Program of the Chinese Academy of Sciences (XDB 12030100).

Received: March 31, 2015
Revised: May 2, 2015
Published online: June 12, 2015

[1] K. S. Novoselov, A. K. Geim, S. V. Morozov, D. Jiang, M. I. Katsnelson, I. V. Grigorieva, S. V. Dubonos, A. A. Firsov, *Nature* **2005**, *438*, 197.
[2] Y. B. Zhang, J. W. Tan, H. L. Stormer, P. Kim, *Nature* **2005**, *438*, 201.
[3] J. H. Chen, C. Jang, S. D. Xiao, M. Ishigami, M. S. Fuhre, *Nat. Nanotechnol.* **2008**, *3*, 206.
[4] K. I. Bolotina, K. J. Sikesb, Z. Jiang, M. Klimac, G. Fudenberg, J. Hone, P. Kim, H. L. Stormer, *Solid State Commun.* **2008**, *146*, 351.
[5] R. Van Noorden, *Nature* **2006**, *442*, 228.
[6] Y. Kobayashi, K. Fukui, T. Enoki, K. Kusakabe, Y. Kaburagi, *Phys. Rev. B* **2005**, *71*, 193406.
[7] Y. Son, M. L. Cohen, S. G. Louie, *Phys. Rev. Lett.* **2006**, *97*, 216803.
[8] Y. Son, M. L. Cohen, S. G. Louie, *Nature* **2006**, *444*, 347.
[9] F. Schedin, A. K. Geim, S. V. Morozov, E. W. Hill, P. Blake, M. I. Katsnelson, K. S. Novoselov, *Nat. Mater.* **2007**, *6*, 652.
[10] A. George, S. Mathew, R. Gastel, M. Nijland, K. Gopinadhan, P. Brinks, T. Venkatesan, J. E. Elshof, *Small* **2013**, *9*, 711.
[11] Y. Pak, H. Jeong, K. H. Lee, H. Song, T. Kwon, J. Park, W. Park, M. S. Jeong, T. Lee, S. Seo, G. Y. Jung, *Adv. Mater.* **2013**, *25*, 199.
[12] Z. W. Shi, R. Yang, L. C. Zhang, Y. Wang, D. H. Liu, D. X. Shi, E. G. Wang, G. Y. Zhang, *Adv. Mater.* **2011**, *23*, 3061.
[13] L. J. Ci, Z. P. Xu, L. L. Wang, W. Gao, F. Ding, K. F. Kelly, B. I. Yakobson, P. M. Ajayan, *Nano Res.* **2008**, *1*, 116.
[14] S. S. Datta, D. R. Strachan, S. M. Khamis, A. T. C. Johnson, *Nano Lett.* **2008**, *8*, 1912.
[15] L. C. Campos, V. R. Manfrinato, J. D. Sanchez-Yamagishi, J. Kong, P. Jarillo-Herrero, *Nano Lett.* **2009**, *9*, 2600.
[16] Y. Zhang, Z. Li, P. Kim, L. Zhang, C. W. Zhou, *ACS Nano* **2012**, *6*, 126.
[17] D. C. Geng, B. Wu, Y. L. Guo, B. R. Luo, Y. Z. Xue, J. Y. Chen, G. Yu, Y. Q. Liu, *J. Am. Chem. Soc.* **2013**, *135*, 6431.
[18] X. F. Zhang, J. Ning, X. L. Li, B. Wang, L. Hao, M. H. Liang, M. H. Jin, L. J. Zhi. *Nanoscale* **2013**, *5*, 8363.
[19] T. Ma, W. Ren, X. Y. Zhang, Z. B. Liu, Y. Gao, L. C. Yin, X. L. Ma, F. Ding, H. M. Cheng. *Proc. Natl. Acad. Sci. USA* **2013**, *110*, 20386.
[20] I. Vlassiouk, M. Regmi, P. Fulvio, S. Dai, P. Datskos, G. Eres, S. Smirnov. *ACS Nano* **2011**, *5*, 6069.
[21] B. Wang, Y. H. Zhang, H. R. Zhang, Z. Y. Chen, X. M. Xie, Y. P. Sui, X. L. Li, G. H. Yu, L. Z. Hu, Z. Jin, X. Y. Liu. *Carbon* **2014**, *70*, 75.
[22] D. C. Geng, B. Wu, Y. L. Guo, L. P. Huang, Y. Z. Xue, J. Y. Chen, G. Yu, L. Jiang, W. P. Hu, Y. Q. Liu, *Proc. Natl. Acad. Sci. USA* **2012**, *109*, 7992.
[23] D. C. Geng, B. R. Luo, J. Xu, Y. L. Guo, B. Wu, W. P. Hu, Y. Q. Liu, G. Yu, *Adv. Funct. Mater.* **2014**, *24*, 1664.
[24] L. Liu, J. Park, D. A. Siegel, K. F. McCarty, K. W. Clark, W. Deng, L. Basile, J. C. Idrobo, A. P. Li, G. Gu, *Science* **2014**, *343*, 163.
[25] V. I. Artyukhov, Y. Liu, B. I. Yakobson, *Proc. Natl. Acad. Sci. USA* **2012**, *109*, 15136.